Advances in Nano Research, *Vol. 17, No.1 (2024) 61-73*
https://doi.org/10.12989/anr.2024.17.1.061

Nonlinear vibration analysis of FG porous shear deformable cylindrical shells covered by CNTs-reinforced nanocomposite layers considering neutral surface exact position

Zhihui Liu*[1,2], Kejun Zhu[1,2], Xue Wen[1,2] and Abhinav Kumar**[3]

[1]*College of Mechanical and Energy Engineering, Shaoyang University, Shaoyang, Hunan, 422000, China*
[2]*Key Laboratory of Hunan Province for Efficient Power System and Intelligent Manufacturing, Shaoyang University, Shaoyang, Hunan, 422000, China*
[3]*Department of Nuclear and Renewable Energy, Ural Federal University Named after the First President of Russia Boris Yeltsin, Ekaterinburg 620002, Russia*

(*Received October 8, 2023, Revised July 12, 2024, Accepted July 16, 2024*)

Abstract. This paper presents nonlinear vibration analysis of a composite cylindrical shell. The core of the shell is made of functionally graded (FG) porous materials and layers is fabricated of carbon nanotubes (CNTs) reinforced nanocomposites. To increase the accuracy of results, neutral surface position is considered. First-order shear deformation theory is used as displacement field to derive the basic relations of equation motions. In addition, von-Karman nonlinear strains are employed to account geometric nonlinearity and to enhance the results' precision, the exact position of the neutral surface is considered. To governing the partial equations of motion, the Hamilton's principle is used. To reduce the equation motions into a nonlinear motion equation, the Galerkin's approach is employed. After that the nonlinear motion equation is solved by multiple scales method. Effect of various parameters such as volume fraction and distribution of CNTs along the thickness directions, different patterns and efficiency coefficients of porous materials, geometric characteristics and initial conditions on nonlinear to linear ratio of frequency is investigated.

Keywords: carbon nanotube reinforcements; cylindrical shells; nonlinear vibration; porous materials; von-Karman strains

1. Introduction

Different shapes of shells, including cylindrical, spherical, conical, and ellipsoidal, have distinct applications and advantages based on their geometrical properties (Gao *et al.* 2022, Wang *et al.* 2023). Cylindrical shells are a type of structural component that finds wide-ranging applications in various fields due to their specific geometrical properties and advantages. Let's explore different shapes of shells, with a focus on cylindrical shells, and discuss their applications and advantages. Cylindrical shells are essentially hollow, tube-like structures with a circular or cylindrical cross-section. They consist of two main components: the outer curved surface and the inner curved surface. These surfaces are typically formed by rolling or bending flat sheets of material. They are commonly used in the construction of pressure vessels, such as boilers and tanks, where they are designed to withstand internal pressure (Han *et al.* 2018, Tian *et al.* 2024, Wang *et al.* 2017). Their curved shape allows them to distribute pressure evenly, making them suitable for containing gases or liquids at high pressures. They are also used in the construction of pipelines for transporting various fluids, including oil, gas, and water. Their streamlined shape reduces fluid resistance, making them energy-efficient for long-distance transport. Cylindrical shells are used as structural components in buildings, bridges, and other engineering structures. They offer high strength-to-weight ratios, allowing for efficient load-bearing capacity. In aerospace engineering, cylindrical shells are used in the construction of aircraft fuselages and rocket casings. Their aerodynamic shape reduces drag and enhances flight performance. Cylindrical tanks are widely used for the storage of liquids and bulk materials. Their cylindrical shape maximizes storage capacity and minimizes material wastage. Consequently, understanding the characteristics of these shell shapes is crucial in engineering and design to select the most appropriate shape for a given application (Dehghan *et al.* 2020, Kalamkarov *et al.* 2006, Kiarasi *et al.* 2021, Mirjavadi *et al.* 2020a, b, Ni *et al.* 2023, Wang *et al.* 2019).

Porous materials, by definition, contain voids or empty spaces within their structure. These voids can range from nanometers to millimeters in size and may be interconnected or isolated. These materials are prized for their unique properties and have a diverse range of applications across various fields. Porosity is the defining characteristic of porous materials. It quantifies the ratio of void volume to total volume and is usually expressed as a percentage. High porosity indicates a larger fraction of empty space within the material. The pore size distribution is a crucial specification, describing the range of pore sizes within the material. This distribution influences properties

*Corresponding author, Ph.D.,
E-mail: hqmx2022@gmail.com
**Co-corresponding author, Ph.D.,
E-mail: drabhinav@ieee.org

ISSN: 2287-237X (Print), 2287-2388 (Online)

like permeability, surface area, and the material's ability to adsorb or release substances. Permeability measures the ease with which fluids or gases flow through the porous material. It depends on both porosity and pore connectivity. Materials with high permeability are valuable for filtration, drainage, or fluid transport applications. Porous materials often exhibit a high surface area due to their numerous pores and internal surfaces. This high surface area is advantageous for applications involving adsorption, catalysis, or gas storage. Bulk density represents the mass of a porous material per unit volume, considering both the solid material and the void spaces. It's a critical specification for structural materials. The mechanical strength of porous materials varies based on composition and fabrication methods. Some are designed to be lightweight with low mechanical strength, while others are engineered for high strength. Porous materials can have unique thermal properties, such as low thermal conductivity, making them suitable for use as insulators or thermal barriers. Chemical reactivity can be tailored by modifying the surface properties of porous materials. Functionalization enhances their ability to adsorb or react with specific substances. In terms of electrical properties, some porous materials exhibit electrical conductivity due to conductive particles within the pores, while others may be insulating or semiconducting. Porous materials have diverse applications in various fields, including catalysis, gas adsorption, water purification, air filtration, biomedical uses (like tissue engineering and drug delivery), energy storage (e.g., batteries and supercapacitors), and construction (for insulation and acoustical control). Researchers and engineers continually explore and develop new porous materials, tailoring their properties for emerging applications in science and technology. These materials, with their versatile characteristics, contribute significantly to advancements across multiple domains (Al-Osta *et al.* 2021, Arefi *et al.* 2019a, Arshid *et al.* 2023a, b, Berghouti *et al.* 2019, Cong *et al.* 2018, Mohammad-Rezaei Bidgoli and Arefi 2019, Mousavi *et al.* 2021, Quang *et al.* 2021, Soleimani-Javid *et al.* 2021, Tahir *et al.* 2021, Zeng *et al.* 2019).

Nanocomposite materials are a class of advanced materials that combine a matrix material with nanoscale reinforcements. These reinforcements can be in the form of nanoparticles, nanofibers, or nanosheets, and they are typically dispersed within the matrix at the nanometer scale (Su *et al.* 2023, Sun *et al.* 2024). The integration of nanoscale reinforcements imparts unique properties to these materials. Nanocomposites feature nanoparticles with dimensions typically ranging from 1 to 100 nanometers. The uniform dispersion of these nanoparticles within the matrix is critical for enhancing material properties. Nanocomposites have a matrix material that can be a polymer, metal, ceramic, or a combination of these. The choice of matrix material depends on the desired properties and application. The nanoscale reinforcements can be of various types, including carbon nanotubes (CNTs), graphene, clay nanoparticles, metal nanoparticles, and more. Each type imparts specific properties to the nanocomposite. Many nanocomposites are lightweight and have a high strength-to-weight ratio, making them ideal for aerospace and automotive applications. Nanocomposite materials find applications in a wide range of industries, including aerospace, automotive, electronics, construction, biomedical, and energy storage. They are used in structural components, coatings, sensors, drug delivery systems, and more (Arefi *et al.* 2018a, Bi *et al.* 2021, Djilali *et al.* 2022, Forsat *et al.* 2021, Paul *et al.* 2013, Safaei *et al.* 2019, Shen *et al.* 2017b, Sobhani *et al.* 2022). The key outstanding characteristics of the FG porous core subjected to compression between CNT-reinforced composite layers, compared to traditional functionally graded materials (FGM), are explained in the following. The addition of CNT reinforcement to the composite layers surrounding the FG porous core provides significant improvements in tensile strength, compressive strength, and impact resistance compared to FGMs without CNT reinforcement (Ninh *et al.* 2023, Ninh and Bich 2016, Tien *et al.* 2021). The CNTs help to effectively transfer and distribute loads through the composite layers (Taj *et al.* 2022, 2023a, b). The FG porous core allows for a more continuous and controllable property gradient to be achieved, compared to the step-wise property changes typical of laminated FGM structures (Babaei *et al.* 2019, 2022, Babaei and Asemi 2022). This enables better optimization of the stress/strain distribution and overall mechanical performance. The porous nature of the core material allows for enhanced energy dissipation and absorption capabilities during compression, impact, or other dynamic loading events. This can make the material more effective for applications like lightweight armor or impact protection. The ability to independently vary the composition and properties of the porous core and the CNT-reinforced composite layers provides greater design flexibility compared to monolithic FGMs. This allows the material properties to be tuned for specific functional requirements. Depending on the specific materials used, the composite structure may also exhibit improved thermal insulation or heat dissipation properties compared to homogeneous FGM counterparts (Arefi *et al.* 2019b, Babaei *et al.* 2024, Bidgoli *et al.* 2022, Khoddami Maraghi and Arshid 2024, Mohammad-Rezaei Bidgoli and Arefi 2023b).

Numerous researches have been conducted by scholars to find out mechanical performance of engineering structures, especially shells that are made from porous and nanocomposite materials (Babaei *et al.* 2020, Bi *et al.* 2023, Kiarasi *et al.* 2020, Shen *et al.* 2024). For instance, in earlier studies, Das (1964) and Dong (1968) investigated the vibrations of orthotropic and laminated orthotropic cylindrical shells. Sivadas and Ganesan (1991) focused on the vibrations of orthotropic shells with variable thickness. Vronay and Smith and (1970) explored the vibrational behavior of finite-length circular cylindrical shells, while Qatu and colleagues (2004, 2010) conducted research on laminated composite shells and plates, examining their dynamic response. Liu *et al.* (2012) discussed the vibrations of orthotropic cylindrical shells. Additionally, various studies have been conducted in the literature on reinforced composites. Shen (2013) delved into FGCNT-reinforced composite plates, considering thermal buckling and post-buckling effects. They factored in temperature variations

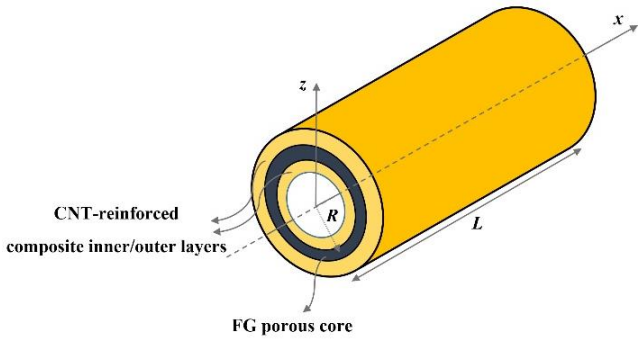

Fig. 1 Schematic of the under-evaluation sandwich composite shell

affecting single-walled carbon nanotubes (SWCNTs) properties and employed a multi-scale approach to obtain their results. Wang and Shen (2012) investigated the impact of thermal conditions on the dynamic response of CNT-reinforced composite plates, considering two CNTs distribution patterns and observing that increased CNTs volume fractions led to higher natural frequencies. Malekzadeh and Shojaee (2013) explored the buckling of quadrilateral laminated plates with CNT-reinforced composite layers. Aragh *et al*. (2012) employed the 2D generalized differential quadrature method to analyze the vibration of continuously graded CNT-reinforced cylindrical panels under various boundary conditions. Jam *et al*. (2012) utilized 3D elasticity to study the vibration of CNTRCs panels, taking into account the aspect ratio and waviness of CNTs. Mohammadimehr and co-authors (2016, 2019) investigated CNT-reinforced composite extensively, considering them as face sheets in sandwich structures. They examined temperature-dependent properties, small-scale behavior, and the impact of electric and magnetic fields on CNT-reinforced composite, presenting their findings and discussing the effects of different parameters. Yas *et al*. (2013) conducted a vibrational analysis of CNT-reinforced composite panels using 3D elasticity, comparing different CNTs distribution patterns within the panels. Shen and his co-authors in different works (Shen and Xiang 2014, Shen 2011, Shen *et al.* 2017a, Shen and Xiang 2013) contributed research on post-buckling and nonlinear vibration of CNT-reinforced composite shells and panels, considering both thermal and mechanical buckling. Shen and Xiang (2014) studied the vibrations of CNT-reinforced composite cylindrical panels with large amplitude deflections, employing the higher-order shear deformation theory for accurate results. This theory is particularly useful for thick structures due to its consideration of shear deformation effects, albeit resulting in more complex equations. Finally, Arshid *et al*. (2022) recently conducted an analysis of higher-order hygro-magneto-electro-thermo-mechanical behavior in FG nanocomposite cylindrical shells with piezo-electro-magnetic layers, with a focus on linearity in their work.

Informed by previous research efforts, this paper aims to advance the understanding of sandwich cylindrical shells and explores their nonlinear vibrational characteristics. It's worth noting that within the realm of published studies, this research constitutes a pioneering analysis of such structures. To align our findings more closely with practicality and harmonize them with experimental studies, the FSDT is employed to model various arbitrary points within the structure. The core of this cylindrical shell is composed of FG porous materials, reinforced with CNT-embedded nano-composite layers to enhance its mechanical performance. The nonlinear governing motion equations are derived using Hamilton's principle. Mathematical solutions for the sandwich cylindrical shell are obtained through the application of Galerkin's and multiple-scale methods. The robustness of our results is substantiated by conducting a comprehensive comparison with prior research findings. The implications of our outcomes span multiple disciplines, including aerospace, automotive, civil engineering, mechanical engineering, and nanotechnology. These findings offer valuable insights into the vibrational behavior of such structures, which are of significant relevance in various real-world applications.

2. Model's description

In this section, the current model under examination is introduced. Fig. 1 displays a cylindrical shell comprising a sandwich structure, where an FG porous core is subjected to compression between layers composed of CNT-reinforced composite materials. The geometric components are depicted in the figure. For context, the entire assembly is assumed to be positioned on a Pasternak elastic foundation. Notations such as h_c, h_t, and h_b are used to represent the thickness of the porous core, top face sheet, and bottom face sheet, respectively. The total thickness, denoted as h_{Total}, is calculated as the sum of h_t, h_c, and h_b. The Cartesian coordinate system (x, y, z), as shown in Fig. 1, is employed for this analysis. Furthermore, the model's geometric properties encompass dimensions such as length (a), width (b), and curvature radius (R). It is important to note that throughout our analysis, a perfect bond is assumed between all three layers, indicating complete adhesion among them.

To enhance precision, the FSDT is employed for characterizing the displacement field within the sandwich model. According to this theory, it becomes feasible to represent the displacements at arbitrary points, whether situated within the FG porous core or the nanocomposite layers, in the following manner (Mindlin 1968):

$$\begin{aligned} u(x,y,z,t) &= u_0(x,y,t) + z\varphi_x(x,y,t) \\ v(x,y,z,t) &= v_0(x,y,t) + z\varphi_y(x,y,t) \\ w(x,y,z,t) &= w_0(x,y,t) \end{aligned} \tag{1}$$

In this context, u, v, and w symbolize the displacements in the x-direction, y-direction, and the transverse displacement along the z-direction, respectively. Moreover, θ_x and θ_y refer to the rotations of the mid-plane around the y and x axes, respectively.

Employing von-Karman's assumptions, utilizing the previously mentioned displacement field, and accounting for nonlinearity, the strain field can be defined as follows (Mao and Zhang 2019):

$$\varepsilon_{xx} = \frac{\partial u}{\partial x} + \frac{1}{2}\left(\frac{\partial w_0}{\partial x}\right)^2 = \frac{\partial u_0}{\partial x} + z\frac{\partial \varphi_x}{\partial x} + \frac{1}{2}\left(\frac{\partial w_0}{\partial x}\right)^2, \tag{2}$$

$$\varepsilon_{yy} = \frac{\partial v}{\partial y} + \frac{\mathrm{w}}{R} + \frac{1}{2}\left(\frac{\partial w_0}{\partial y}\right)^2 = \frac{\partial v_0}{\partial y} + z\frac{\partial \varphi_y}{\partial y} + \frac{w_0}{R} + \frac{1}{2}\left(\frac{\partial w_0}{\partial y}\right)^2,$$

$$\gamma_{xy} = \frac{\partial v}{\partial x} + \frac{\partial \mathrm{u}}{\partial y} + \frac{\partial w_0}{\partial x}\frac{\partial w_0}{\partial y} = \frac{\partial v_0}{\partial x} + z\frac{\partial \varphi_y}{\partial x} + \frac{\partial u_0}{\partial y} + z\frac{\partial \varphi_x}{\partial y} + \frac{\partial w_0}{\partial x}\frac{\partial w_0}{\partial y},$$

$$\gamma_{xz} = \frac{\partial u}{\partial z} + \frac{\partial \mathrm{w}}{\partial x} = \varphi_x + \frac{\partial w_0}{\partial x},$$

$$\gamma_{yz} = \frac{\partial v}{\partial z} + \frac{\partial \mathrm{w}}{\partial y} - \frac{\mathrm{v}}{R} = \varphi_y + \frac{\partial w_0}{\partial y} - \frac{v_0}{R} - \frac{z}{R}\varphi_y$$

In this study, the precise position of the shell's neutral surface is determined and then employed in the subsequent relationships. This positioning is achieved to ensure satisfaction of the following equation (Radić 2018):

$$\int_{-\frac{h_{Total}}{2}}^{\frac{h_{Total}}{2}} c_{11}(z - C)\,\mathrm{dz} = 0 \tag{3}$$

Here C denoting the distance of the neutral surface position from the mid-surface of the shell, can be determined by:

$$C = \frac{\int_{-\frac{h_{Total}}{2}}^{\frac{h_{Total}}{2}} c_{11} z\,\mathrm{dz}}{\int_{-\frac{h_{Total}}{2}}^{\frac{h_{Total}}{2}} c_{11}\,\mathrm{dz}} \tag{4}$$

The stress-strain relationships for both the FG porous core and CNT-reinforced composite layers are articulated as follows (Alhaifi *et al.* 2023, Kaveh *et al.* 2024):

$$\begin{bmatrix}\sigma_{xx}\\ \sigma_{yy}\\ \sigma_{yz}\\ \sigma_{xz}\\ \sigma_{xy}\end{bmatrix} = \begin{bmatrix} Q_{11} & Q_{12} & 0 & 0 & 0\\ Q_{21} & Q_{22} & 0 & 0 & 0\\ 0 & 0 & Q_{44} & 0 & 0\\ 0 & 0 & 0 & Q_{55} & 0\\ 0 & 0 & 0 & 0 & Q_{66}\end{bmatrix}^{c,f} \begin{Bmatrix}\varepsilon_{xx}\\ \varepsilon_{yy}\\ \gamma_{yz}\\ \gamma_{xz}\\ \gamma_{xy}\end{Bmatrix} \tag{5}$$

The elastic coefficients, denoted as c_{ij}, are specified individually for both the FG porous core and the CNT-reinforced composite layers, and the superscripts c and f denote the core and face sheets.

3. Nonlinear governing motion equations

The derivation of the nonlinear governing equations of motion utilizes Hamilton's principle, which takes into account the energies associated with strain and kinetic components as well as external work. This principle can be formally presented as follows (Arshid *et al.* 2024a, Jalaei and Civalek 2019):

$$\delta \int_{t_1}^{t_2} (U - K - V)\mathrm{d}t = 0 \tag{6}$$

In this context, U, T, and W represent the strain energy, kinetic energy, and external work, respectively. It is important to highlight that in this paper, the Pasternak foundation is assumed to bear the weight of the sandwich model. This foundation has the unique capability to simulate both transverse and normal loads. The force exerted on the sandwich model by the foundation can be formally presented as follows (Arefi *et al.* 2018b, Mohammad-Rezaei Bidgoli and Arefi 2023c):

$$F_f = k_1 w_0 - k_2\left(\frac{\partial^2 w_0}{\partial x^2} + \frac{\partial^2 w_0}{\partial y^2}\right) \tag{7}$$

The Winkler constant, symbolized as k_1, and the shear layer parameter, designated as k_2, characterize the characteristics of the Pasternak substrate. Consequently, the changes in external work induced by the presence of the Pasternak substrate can be formally articulated as follows (Arshid *et al.* 2022, 2024b):

$$\delta V = \int_A -F_f\left(1 - \frac{h}{2R}\right)\delta w_0 \mathrm{d}A \tag{8}$$

Next, the focus shifts to the calculation of strain energy and its variations. The strain energy of the model under examination is defined as follows (Zavari *et al.* 2024):

$$\delta U = \iiint_V (\sigma_{ij}\delta\varepsilon_{ij})\mathrm{d}V \tag{9}$$

Its variation is determined as follows:

$$\delta U = \iiint_V \begin{pmatrix}\sigma_{xx}\delta\varepsilon_{xx} + \sigma_{yy}\delta\varepsilon_{yy} + \sigma_{yz}\delta\gamma_{yz}\\ +\sigma_{xz}\delta\gamma_{xz} + \sigma_{xy}\delta\gamma_{xy}\end{pmatrix}\mathrm{d}V \tag{10}$$

By inserting the obtained strains into the equation mentioned above, the following expression is derived:

$$\delta U = \iiint_V \begin{bmatrix} \sigma_{xx}\left(\frac{\partial \delta u_0}{\partial x} + z\frac{\partial \delta\varphi_x}{\partial x} + \frac{\partial w_0}{\partial x}\frac{\partial \delta w_0}{\partial x}\right)\\ +\sigma_{yy}\left(\frac{\partial \delta v_0}{\partial y} + z\frac{\partial \delta\varphi_y}{\partial y} + \frac{\delta w_0}{R} + \frac{\partial w_0}{\partial y}\frac{\partial \delta w_0}{\partial y}\right)\\ +\sigma_{yz}\left(\delta\varphi_y + \frac{\partial \delta w_0}{\partial y} - \frac{\delta v_0}{R} - \frac{z}{R}\delta\varphi_y\right)\\ +\sigma_{xz}\left(\delta\varphi_x + \frac{\partial \delta w_0}{\partial x}\right)\\ +\sigma_{xy}\begin{pmatrix}\frac{\partial \delta v_0}{\partial x} + z\frac{\partial \delta\varphi_y}{\partial x} + \frac{\partial \delta u_0}{\partial y} + z\frac{\partial \delta\varphi_x}{\partial y}\\ +\frac{\partial \delta w_0}{\partial x}\frac{\partial w_0}{\partial y} + \frac{\partial w_0}{\partial x}\frac{\partial \delta w_0}{\partial y}\end{pmatrix}\end{bmatrix} dV \tag{11}$$

Through the separation of integrals with respect to z and the establishment of stress resultants, in addition to the application of variational formulations, we arrive at the following expression for the variations in strain energy:

$$\delta U = \iint_A \begin{bmatrix} \left(-\frac{\partial H_{xx}}{\partial x} - \frac{\partial H_{xy}}{\partial y}\right)\delta u_0\\ +\left(-\frac{\partial H_{yy}}{\partial y} - J_{yz} - \frac{\partial H_{xy}}{\partial x}\right)\delta v_0\\ \begin{pmatrix}-\frac{\partial}{\partial x}\left(H_{xx}\frac{\partial w_0}{\partial x}\right) + J_{yy}\\ -\frac{\partial}{\partial y}\left(H_{yy}\frac{\partial w_0}{\partial y}\right) - \frac{\partial H_{yz}}{\partial y} - \frac{\partial H_{xz}}{\partial x}\\ -\frac{\partial}{\partial x}\left(H_{xy}\frac{\partial w_0}{\partial y}\right) - \frac{\partial}{\partial y}\left(H_{xy}\frac{\partial w_0}{\partial x}\right)\end{pmatrix}\delta w_0\\ +\left(-\frac{\partial G_{xx}}{\partial x} + H_{xz} - \frac{\partial G_{xy}}{\partial y}\right)\delta\varphi_x\\ +\left(-\frac{\partial G_{yy}}{\partial y} + H_{yz} - G_{yz} - \frac{\partial G_{xy}}{\partial x}\right)\delta\varphi_y\end{bmatrix}\mathrm{d}A \tag{12}$$

in which:

$$(H_{xx}, G_{xx}) = \int_{-\frac{h_c}{2}-h_b-C}^{-\frac{h_c}{2}-C} \sigma_{xx}^{b}(1,z)\,\mathrm{d}z + \int_{-\frac{h_c}{2}-C}^{+\frac{h_c}{2}-C} \sigma_{xx}^{c}(1,z)\,\mathrm{d}z + \int_{+\frac{h_c}{2}-C}^{+\frac{h_c}{2}+h_t-C} \sigma_{xx}^{t}(1,z)\,\mathrm{d}z, \tag{13}$$

$$\left(H_{yy}, G_{yy}, J_{yy}\right) = \int_{-\frac{h_c}{2}-h_b-C}^{-\frac{h_c}{2}-C} \sigma_{yy}^{b}\left(1,z,\frac{1}{R}\right)\mathrm{d}z + \int_{-\frac{h_c}{2}-C}^{+\frac{h_c}{2}-C} \sigma_{yy}^{c}\left(1,z,\frac{1}{R}\right)\mathrm{d}z + \int_{+\frac{h_c}{2}-C}^{+\frac{h_c}{2}+h_t-C} \sigma_{yy}^{t}\left(1,z,\frac{1}{R}\right)\mathrm{d}z, \tag{14}$$

$$\left(H_{yz}, G_{yz}, J_{yz}\right) = \int_{-\frac{h_c}{2}-h_b-C}^{-\frac{h_c}{2}-C} k_s\sigma_{yz}^{b}\left(1,\frac{z}{R},\frac{1}{R}\right)\mathrm{d}z + \int_{-\frac{h_c}{2}-C}^{+\frac{h_c}{2}-C} k_s\sigma_{yz}^{c}\left(1,\frac{z}{R},\frac{1}{R}\right)\mathrm{d}z + \int_{+\frac{h_c}{2}-C}^{+\frac{h_c}{2}+h_t-C} k_s\sigma_{yz}^{t}\left(1,\frac{z}{R},\frac{1}{R}\right)\mathrm{d}z, \tag{15}$$

$$H_{xz} = \int_{-\frac{h_c}{2}-h_b-C}^{-\frac{h_c}{2}-C} k_s\sigma_{xz}^{b}\,\mathrm{d}z + \int_{-\frac{h_c}{2}-C}^{+\frac{h_c}{2}-C} k_s\sigma_{xz}^{c}\,\mathrm{d}z + \int_{+\frac{h_c}{2}-C}^{+\frac{h_c}{2}+h_t-C} k_s\sigma_{xz}^{t}\,\mathrm{d}z, \tag{16}$$

$$\left(H_{xy}, G_{xy}\right) = \int_{-\frac{h_c}{2}-h_b-C}^{-\frac{h_c}{2}-C} \sigma_{xy}^{b}(1,z)\,\mathrm{d}z + \int_{-\frac{h_c}{2}-C}^{+\frac{h_c}{2}-C} \sigma_{xy}^{c}(1,z)\,\mathrm{d}z + \int_{+\frac{h_c}{2}-C}^{+\frac{h_c}{2}+h_t-C} \sigma_{xy}^{t}(1,z)\,\mathrm{d}z \tag{17}$$

In the above relations, k_s is the shear correction factor of FSDT. On the other hand, in order to calculate the kinetic energy of the sandwich shell, the following formula can be applied (Arshid *et al.* 2024c, Kargar *et al.* 2021, Zhao *et al.* 2019):

$$\int_{t_1}^{t_2} K\mathrm{d}t = \int_{t_1}^{t_2} \iiint_{V} \rho(z)\left(\frac{\partial u_i}{\partial t}\right)^2 \mathrm{d}V\mathrm{d}t \tag{18}$$

Regarding the defined displacements in Eq. (1), variations of the kinetic energy may be written as:

$$\int_{t_1}^{t_2} \delta K\, dt \tag{19}$$

$$= \int_{t_1}^{t_2} \iint_{A} \begin{bmatrix} \left(-I_0\frac{\partial^2 u_0}{\partial t^2} - I_1\frac{\partial^2 \varphi_x}{\partial t^2}\right)\delta u_0 \\ +\left(-I_0\frac{\partial^2 v_0}{\partial t^2} - I_1\frac{\partial^2 \varphi_y}{\partial t^2}\right)\delta v_0 \\ +\left(-I_0\frac{\partial^2 w_0}{\partial t^2}\right)\delta w_0 \\ +\left(-I_1\frac{\partial^2 u_0}{\partial t^2} - I_2\frac{\partial^2 \varphi_x}{\partial t^2}\right)\delta \varphi_x \\ +\left(-I_1\frac{\partial^2 v_0}{\partial t^2} - I_2\frac{\partial^2 \varphi_y}{\partial t^2}\right)\delta \varphi_y \end{bmatrix} \mathrm{d}A\mathrm{d}t$$

where:

$$(I_0, I_1, I_2) = \int_{-\frac{h_c}{2}-h_b-C}^{-\frac{h_c}{2}-C} \rho^{b}(1,z,z^2)\,\mathrm{d}z + \int_{-\frac{h_c}{2}-C}^{+\frac{h_c}{2}-C} \rho^{c}(1,z,z^2)\,\mathrm{d}z + \int_{+\frac{h_c}{2}-C}^{+\frac{h_c}{2}+h_t-C} \rho^{t}(1,z,z^2)\,\mathrm{d}z \tag{20}$$

In this case, applying Hamilton's principle and considering the obtained expressions for variations in strain and kinetic energies, as well as the inclusion of external work, results in the extraction of the following set of five nonlinear differential governing equations of motion:

$$\delta u_0 : \frac{\partial H_{xx}}{\partial x} + \frac{\partial H_{xy}}{\partial y} = I_0\frac{\partial^2 u_0}{\partial t^2} + I_1\frac{\partial^2 \varphi_x}{\partial t^2}, \tag{21}$$

$$\delta v_0 : \frac{\partial H_{yy}}{\partial y} + J_{yz} + \frac{\partial H_{xy}}{\partial x} = I_0\frac{\partial^2 v_0}{\partial t^2} + I_1\frac{\partial^2 \varphi_y}{\partial t^2}, \tag{22}$$

$$\begin{aligned} \delta w_0 : {} & \frac{\partial}{\partial x}\left(H_{xx}\frac{\partial w_0}{\partial x}\right) + \frac{\partial}{\partial y}\left(H_{yy}\frac{\partial w_0}{\partial y}\right) + \frac{\partial}{\partial x}\left(H_{xy}\frac{\partial w_0}{\partial y}\right) \\ & + \frac{\partial}{\partial y}\left(H_{xy}\frac{\partial w_0}{\partial x}\right) + \frac{\partial H_{yz}}{\partial y} + \frac{\partial H_{xz}}{\partial x} - J_{yy} - F_f\left(1 - \frac{h}{2R}\right) \\ & = I_0\frac{\partial^2 w_0}{\partial t^2}, \end{aligned} \tag{23}$$

$$\delta \varphi_x : \frac{\partial G_{xx}}{\partial x} + \frac{\partial G_{xy}}{\partial y} - H_{xz} = I_1\frac{\partial^2 u_0}{\partial t^2} + I_2\frac{\partial^2 \varphi_x}{\partial t^2}, \tag{24}$$

$$\delta \varphi_y : \frac{\partial G_{yy}}{\partial y} + \frac{\partial G_{xy}}{\partial x} - H_{yz} + G_{yz} = I_1\frac{\partial^2 v_0}{\partial t^2} + I_2\frac{\partial^2 \varphi_y}{\partial t^2} \tag{25}$$

4. Materials properties

Attention is now directed to the inner and outer layers, which are constructed using CNT-reinforced composite materials. These layers are composed of a polymer matrix with CNT fibers serving as the reinforcing phase. The elastic coefficients for these layers are defined as follows (Arshid *et al.* 2023c, Bidgoli and Arefi 2023):

$$Q_{11}^{f} = \frac{E_{11}}{1-\nu_{12}\nu_{21}}, \qquad Q_{22}^{f} = \frac{E_{22}}{1-\nu_{12}\nu_{21}}, \tag{26}$$

$$Q_{12}^f = \nu_{21} Q_{11}^f, \qquad Q_{44}^f = G_{23},$$

$$Q_{55}^f = G_{13}, \qquad Q_{66}^f = G_{12}$$

Here, it's important to highlight that the knowledge of the mechanical properties of the composite layer is imperative for the mathematical derivation and solution of the governing equations. To achieve this, the extended rule of mixture (ERM) is employed to combine the mechanical properties of the matrix and reinforcing phases, thereby establishing the mechanical properties of the entire composite layer. In accordance with the ERM approach, the material properties of the nanocomposite layers are as follows (Allahkarami *et al*. 2018, Arshid *et al.* 2023d):

$$\nu_{12} = V_{main}^{CNT} \nu_{12}^{CNT} + V^P \nu^P, \tag{27}$$

$$\rho_c = V^{CNT} \rho^{CNT} + V^P \rho^P, \tag{28}$$

$$E_{11} = \eta_1 V^{CNT} E_{11}^{CNT} + V^P E^P, \tag{29}$$

$$\frac{\eta_3}{G_{12}} = \frac{V^{CNT}}{G_{12}^{CNT}} + \frac{V^P}{G^P}, \qquad \frac{\eta_2}{E_{22}} = \frac{V^{CNT}}{E_{22}^{CNT}} + \frac{V^P}{E^P} \tag{30}$$

In these equations, the letter *P* signifies the polymeric matrix, and η_k (where *k* takes on values of 1, 2, and 3) represents the CNT efficiency parameter. It's important to note that η_k depends on the total volume of CNTs present in the composite material, as detailed in Table 1 (Jeyaraj and Rajkumar 2013).

V^P represents the volume fraction for the matrix, while V^{CNT} stands for the volume fraction pertaining to the CNTs. It's essential to emphasize that the sum of V^P and V^{CNT} must equal 1, indicating the entirety of the material composition.

Furthermore, it's crucial to distinguish V^{CNT} from $V^{CNT}{}_{\text{main}}$ as V^{CNT} is dependent on the dispersion pattern of CNTs within the polymer matrix phase. In other words, V^{CNT} varies based on the CNT dispersion pattern. The expressions for V^{CNT} and $V^{CNT}{}_{\text{main}}$ can be formulated as follows (Amir *et al.* 2020a):

$$V_{main}^{CNT} = \frac{w^{CNT}}{w^{CNT} + (\rho^{CNT}/\rho^P) - (\rho^{CNT}/\rho^P) w^{CNT}} \tag{31}$$

$$V_i^{CNT} = \begin{cases} V_{main}^{CNT} & FG-UU \\ \left[1 - \frac{2}{h_i}\left(z \pm \frac{h_c + h_i}{2}\right)\right] V_{main}^{CNT} & FG-AV \\ \left[1 + \frac{2}{h_i}\left(z \pm \frac{h_c + h_i}{2}\right)\right] V_{main}^{CNT} & FG-VA \\ 2\left[1 - \frac{2}{h_i}\left(z \pm \frac{h_c + h_i}{2}\right)\right] V_{main}^{CNT} & FG\text{-}OO \\ \left[\frac{4}{h_i}\left(\left|z \pm \frac{h_c + h_i}{2}\right|\right)\right] V_{main}^{CNT} & FG\text{-}XX \end{cases} \quad i = t, b \tag{32}$$

In the equations mentioned above, the subscripts 't' and 'b' are abbreviations for 'Top' and 'Bottom,' respectively, arranged sequentially. Additionally, *w* signifies the mass fraction, while FG-AV, FG-VA, FG-OO, and FG-XX indicate the dispersion patterns of CNTs within the matrix phase. Specifically, 'UU' represents the uniform dispersion pattern.

Table 1 Efficiency parameters of CNTs (Jeyaraj and Rajkumar 2013)

V_{main}^{CNT}	η_1	η_2	η_3
0.12	0.137	1.022	0.715
0.17	0.142	1.626	1.138
0.28	0.141	1.585	1.109

Now, let's delve into the definitions of elastic coefficients for the FG porous core. As highlighted in the previous section, a porous layer serves as the core of the aforementioned sandwich cylindrical shell. Consequently, the elastic coefficients are assumed to have the following values (Amir *et al.* 2020b, Khoddami Maraghi *et al.* 2022):

$$\begin{aligned} Q_{11}^c &= Q_{22}^c = \frac{E_c(z)}{1 - \nu_c^2}, \\ Q_{12}^c &= \frac{\nu_c E_c(z)}{1 - \nu_c^2}, \\ Q_{ii}^c &= G_c(z), \qquad i = 4,5,6 \end{aligned} \tag{33}$$

in which $E_c(z)$, $G_c(z)$, and ν_c indicate elastic modulus, shear modulus and Poisson's ratio of the FG porous core, respectively.

The elastic constants of the core shell are influenced by the type of porosity distribution within it, leading to variations in both the elastic modulus and core density. Among the three established types of porosity distribution (uniform, non-uniform, and even), this paper focuses on the non-uniform distribution, specifically termed "Distribution 1". Under this condition, the following relationships define the elastic constants (Qin *et al.* 2020):

$$E_c(z) = E_0 \left[1 - e_0 \cos\left(\left\{\frac{\pi}{2h_c}\left(z + \frac{h_c}{2}\right)\right\}\right)\right], \tag{34}$$

$$\rho_c(z) = \rho_0 \left[1 - e_m \cos\left(\left\{\frac{\pi}{2h_c}\left(z + \frac{h_c}{2}\right)\right\}\right)\right], \tag{35}$$

$$e_m = 1 - \sqrt{1 - e_0} \tag{36}$$

These relationships are expressed in terms of e_0 which represents the porosity coefficient, and e_m which is the mass density factor. In the "Distribution 2" pattern, it's noteworthy that there is an independence of thickness parameters in the modulus and density equations, which is associated with uniform porosity distribution (Hou *et al.* 2023):

$$E_c(z) = E_0[1 - e_0 \zeta], \tag{37}$$

$$\rho_c(z) = \rho_0 \sqrt{1 - e_0 \zeta}, \tag{38}$$

$$\zeta = \frac{1}{e_0} - \frac{1}{e_0}\left(\frac{2}{\pi}\sqrt{1 - e_0} - \frac{2}{\pi} + 1\right)^2 \tag{39}$$

In the scenario of even porosity distribution, referred to as "Distribution 3," pores are symmetrically distributed across the porous layer. The corresponding distribution of elastic modulus and density can be defined as follows:

Table 2 Material properties of the CNT-reinforced composite layers (Alibeigloo 2013)

Properties	*SWCNTs*	*PVDF*
v	0.175	0.34
ρ (kg/m^3)	1400	1150
E_{11} (TPa)	5.6466	E_m (GPa)= 2.5
$E_{22}=E_{33}$(TPa)	7.0800	
$G_{12}=G_{23}=G_{13}$	1.9445	

Table 3 Validation the results in simpler case with previously published work.

R/a	Source	k				
		0.5	1	2	5	10
5	Kiani *et al.* (2012)	7.0497	6.7171	6.4280	6.1525	5.9721
	Present	7.0716	6.7387	6.4354	6.1720	5.9773
10	Kiani *et al.* (2012)	5.8314	5.5586	5.3502	5.1711	5.0285
	Present	5.8492	5.5729	5.3624	5.1843	5.0494
20	Kiani *et al.* (2012)	5.4839	5.2282	5.0442	4.8944	4.7629
	Present	5.4936	5.2376	5.0527	4.9018	4.7748

$$E_c(z) = E_0\left[1 - e_0\cos\left(\frac{\pi z}{h_c}\right)\right], \tag{40}$$

$$\rho_c(z) = \rho_0\left[1 - e_m\cos\left(\frac{\pi z}{h_c}\right)\right] \tag{41}$$

In the aforementioned equations, it's important to note that E_0 represents the maximum elastic modulus, while ρ_0 stands for the maximum density within the FG porous core.

5. Semi-analytical solution process

The nonlinear governing equations of motion under simply supported boundary conditions are effectively solved through the application of Galerkin's method in conjunction with the multiple scale method. In this context, the following functions are defined (Mohammad-Rezaei Bidgoli and Arefi 2023a):

$$\begin{aligned}
u_0(x,y,t) &= \sum_{m=1}^{\infty}\sum_{n=1}^{\infty}\widetilde{U}_{mn}(t)\cos(\alpha x)\sin(\beta y),\\
v_0(x,y,t) &= \sum_{m=1}^{\infty}\sum_{n=1}^{\infty}\widetilde{V}_{mn}(t)\sin(\alpha x)\cos(\beta y),\\
w_0(x,y,t) &= \sum_{m=1}^{\infty}\sum_{n=1}^{\infty}\widetilde{W}_{mn}(t)\sin(\alpha x)\sin(\beta y),\\
\varphi_x(x,y,t) &= \sum_{m=1}^{\infty}\sum_{n=1}^{\infty}\widetilde{N}_{mn}(t)\cos(\alpha x)\sin(\beta y),\\
\varphi_y(x,y,t) &= \sum_{m=1}^{\infty}\sum_{n=1}^{\infty}\widetilde{D}_{mn}(t)\sin(\alpha x)\cos(\beta y)
\end{aligned} \tag{42}$$

Here, where β is defined as $n\pi/b$, and α is represented as $m\pi/a$. The coefficients $\widetilde{U}$, $\widetilde{V}$, $\widetilde{W}$, $\widetilde{N}$, and $\widetilde{D}$ represent the unknowns in this context. The values (m,n) correspond to the mode numbers along the x and y directions. Upon substituting these solutions into the governing equations of motion and subsequently applying Galerkin's method (Dzung *et al.* 2024, Ha *et al.* 2024), taking certain assumptions into account, the final governing equation of motion in the time domain is obtained as follow:

$$\frac{d^2\widetilde{W}_{mn}(t)}{dt^2} + \alpha_1\widetilde{W}_{mn}(t) + \alpha_2\widetilde{W}_{mn}^2(t) + \alpha_3\widetilde{W}_{mn}^3(t) = 0 \tag{43}$$

Also, the initial conditions are as below:

$$\widetilde{W}_{mn}(t=0) = \frac{W_{Max}}{h} = A\,,\quad \frac{d\widetilde{W}_{mn}(t)}{dt}(t=0) = 0 \tag{44}$$

The explicit solution of the nonlinear equations leads to following result (Babaei and Eslami 2021):

$$\frac{\omega_{NL}}{\omega_L} = \left[1 + \frac{9\alpha_1\alpha_3 - 10\alpha_2^2}{12\alpha_1^2}A^2\right]^{1/2} \tag{45}$$

6. Debate on the results

This section is dedicated to presenting the results, aiming to offer a comprehensive understanding of the nonlinear vibrational behavior exhibited by the under-evaluation model. The FG porous core has E_c=200×10^9 Pa, ρ_c=7850 kg/m^3, and v_c=0.33. Additionally, Table 2 provides the properties of the matrix (Epoxy) and the reinforcement (CNTs), serving as constituents of the inner and outer layers (Alibeigloo 2013).

To ensure the code's validity and enhance its reliability, results concerning the impacts of geometrical and material properties on linear and normalized natural frequencies were obtained using the current code. These results were subsequently compared with those reported by Kiani *et al.* (2012) in Table 3. This Table presents the results for a/b=1, a/h=50, and various values of the R/a ratio and the material gradient index (k) of FG materials. Upon examination of Table 3, it becomes apparent that the results from the mentioned paper (Kiani *et al.* 2012), while displaying minor differences, can be attributed to different assumptions or the utilization of varying displacement field formulations. Consequently, the code presented in the current paper can be considered reliable, and its results can offer dependable insights into the vibrational behavior of such lightweight structures.

Now it turns to consider the current work's results. The Fig. 2 is presented to study the effect of porosity coefficient and also, W_{Max}/h_{Total} ratio on the nonlinear-to-linear frequency ratio. It is seen that by increasing the porosity coefficient, the results tend to reduce. Increasing porosity typically reduces the effective mass of the shell because voids within the material have less mass compared to the solid material. In structural dynamics, the frequency of a structure is inversely proportional to the square root of its mass. Therefore, a reduction in mass due to increased porosity can lead to a decrease in the frequency. Porous

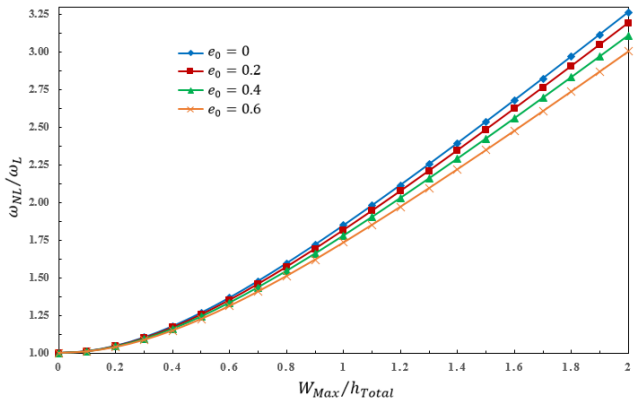

Fig. 2 Effect of porosity coefficient and W_{Max}/h_{Total} ratio on the results

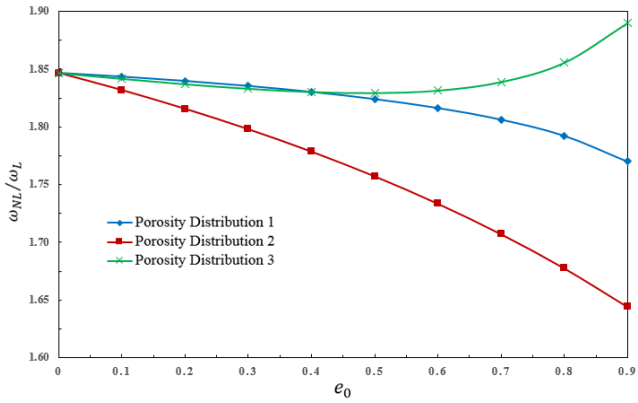

Fig. 3 Impact of porosity coefficient and different types of pores distribution on the results

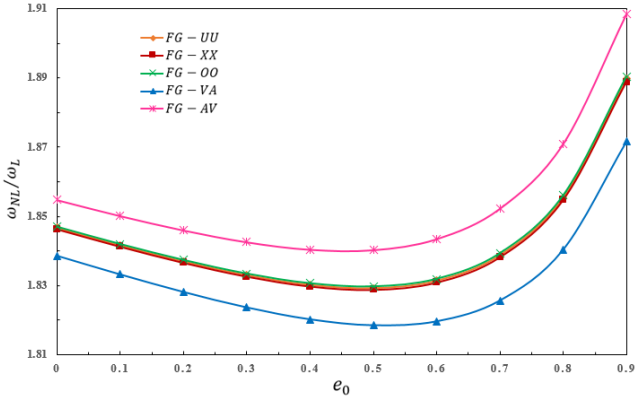

Fig. 4 Influence of porosity coefficient and different pattern of CNTs' dispersion in the inner and outer layer on the frequencies

materials are often less stiff than their solid counterparts. This reduced stiffness can also contribute to a decrease in frequency because stiffness is directly related to the square of the frequency. It's important to note that the exact relationship between porosity and frequency depends on the specific geometry and material properties of the shell, as well as the boundary conditions and the type of vibrations or oscillations under consideration. In some cases, increased porosity may lead to a significant reduction in frequency,

Table 4 Exact values of the results for CNTs' different distribution patterns and W_{Max}/h_{Total} ratio

$\frac{W_{max}}{h_{Total}}$	CNTs Distribution Pattern				
	FG-UU	FG-XX	FG-OO	FG-VA	FG-AV
0	1.0000	1.0000	1.0000	1.0000	1.0000
0.1	1.0107	1.0107	1.0107	1.0104	1.0110
0.2	1.0422	1.0421	1.0422	1.0410	1.0434
0.3	1.0927	1.0926	1.0928	1.0902	1.0953
0.4	1.1597	1.1594	1.1598	1.1555	1.1640
0.5	1.2405	1.2401	1.2407	1.2344	1.2468
0.6	1.3327	1.3322	1.3329	1.3244	1.3410
0.7	1.4340	1.4333	1.4342	1.4235	1.4445
0.8	1.5426	1.5418	1.5429	1.5299	1.5554
0.9	1.6572	1.6562	1.6575	1.6421	1.6722
1	1.7764	1.7753	1.7768	1.7591	1.7938
1.1	1.8996	1.8983	1.9000	1.8800	1.9192
1.2	2.0259	2.0245	2.0263	2.0040	2.0478
1.3	2.1548	2.1533	2.1553	2.1307	2.1790
1.4	2.2859	2.2842	2.2864	2.2595	2.3123
1.5	2.4188	2.4170	2.4193	2.3901	2.4474
1.6	2.5532	2.5512	2.5538	2.5223	2.5840
1.7	2.6889	2.6868	2.6895	2.6558	2.7220
1.8	2.8257	2.8235	2.8264	2.7904	2.8610
1.9	2.9635	2.9611	2.9642	2.9260	3.0010
2	3.1021	3.0996	3.1029	3.0624	3.1418

while in others, the effect may be less pronounced. Also, it is observed that by increasing the W_{Max}/h_{Total} ratio, the results enhance significantly. The following numerical values and specifications are used to extract this figure: $h_c = 0.005m$, $h_b = h_t = 0.001m$, $a = b = 20h_{Total}$, $R = 10a$, $V_{main}^{CNT} = 0.28$, $e_0 = 0.3$, $k_1 = k_2 = 0$, and Distribution 3 of porosity.

Curvatures plotted in Fig. 3 are responsible to examine the impacts of both porosity distribution types and also, coefficient. It is understood that increasing porosity in two types, i.e., Porosity distribution 1 and 2 leads to reduction in the results, while for Porosity distribution 3 that is related to the symmetric pattern, the results enhance a bit. It occurs due to reduction or enhancement in stiffness-to-mass ratio of the shell. The following numerical values and specifications are used to extract this figure:

$h_c = 0.005m$, $h_b = h_t = 0.001m$, $a = b = 20h_{Total}$, $R = 10a$, $V_{main}^{CNT} = 0.12$, $W_{max}/h_{Total} = 1$, $FG-UU$, $k_1 = k_2 = 0$

Results plotted in Fig. 4 can provide a useful physical vision toward different patterns of dispersion of CNT in the inner and outer layers. It is found that FG-AV and FG-VA patterns lead to the most and the least values of the results and the other patterns outcomes are too close to each other. The following numerical values and specifications are used to extract this figure:

$h_c = 0.005m$, $h_b = h_t = 0.001m$, $a = b = 20h_{Total}$, $R = 10a$, $V_{main}^{CNT} = 0.12$,

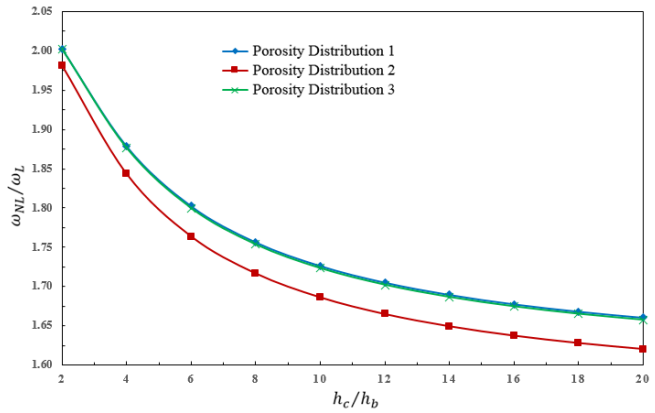

Fig. 5 Effect of layers' thicknesses ratio on the results

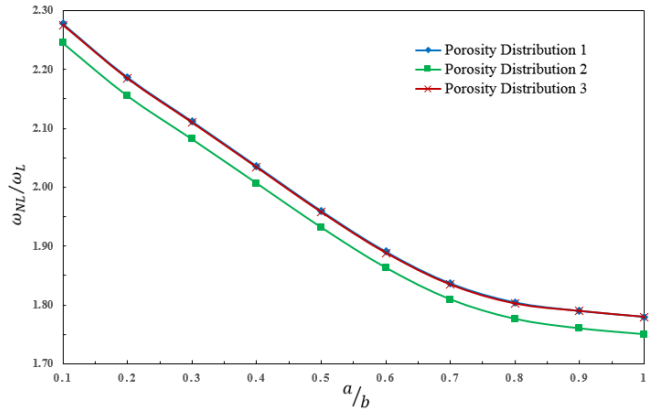

Fig. 6 Effect of geometrical parameters of the shell and porosity distribution on the results

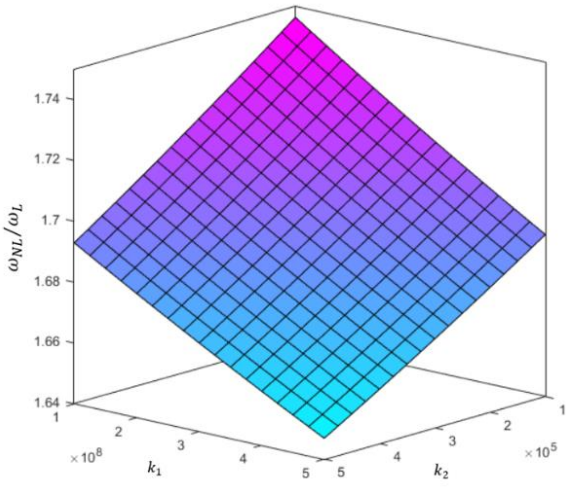

Fig. 7 Impact of Pasternak foundation's parameters on the results

$W_{max}/h_{Total} = 1$, $Porosity\ Distribution\ 3, k_1 = k_2 = 0$

Exact values of the results toward different patterns of CNTs' distribution and also, W_{Max}/h_{Total} ratio are listed in Table 4. This table confirms the previous findings about the effect of CNTs' distribution patterns on the results. The following numerical values and specifications are used to extract this table:

$h_c = 0.005m$, $h_b = h_t = 0.001m$,
$a = b = 20h_{Total}$, $R = 10a$, $V_{main}^{CNT} = 0.28$,
$Porosity\ Distribution\ 3$, $e_0 = 0.3$, $k_1 = k_2 = 0$

Fig. 5 shows the effect of layers' thicknesses ratio on the results. Regarding this figure it can be understood that increasing the core-to-faces thickness ratio leads the results to a reduction. In fact, the stiffness of the inner and outer layers is much more than the FG porous core and by keeping the total thickness constant, increasing the core's thickness means a reduction in inner and outer layers thickness which leads to reduction in stiffness of the whole structure. Therefore, the results are reduced, too. It occurs for all three-porosity distribution pattern that are investigated in this work. The following numerical values and specifications are used to extract this figure:

$a = b = 20h_{Total}$, $R = 10a$, $V_{main}^{CNT} = 0.12$,
$W_{max}/h_{Total} = 1$, $FG - UU$, $k_1 = k_2 = 0$, $e_0 = 0.3$

In Fig. 6, the influence of geometrical parameter of the shell, i.e., its length-to-width ratio is considered and it is seen due to a significant reduction in the shell's stiffness, consequently, the results are reduced. The following numerical values and specifications are used to extract this figure:

$h_c = 0.005m$, $h_b = h_t = 0.001m$, $R = 10a$,
$V_{main}^{CNT} = 0.17$, $W_{max}/h_{Total} = 1$, $FG - UU$,
$k_1 = k_2 = 0, e_0 = 0.3$, $Area = Constant$

And finally in Fig. 7, the effect of Pasternak foundation parameters is observed. As can be expected, increasing both these two parameters, i.e., springs and shear layer parameters, the rigidity of the structure enhance and accordingly, the results are also enhanced. The following numerical values and specifications are used to extract this figure:

$h_c = 0.005m$, $h_b = h_t = 0.001m$, $a = b = 20h_{Total}$,
$R = 10a$, $V_{main}^{CNT} = 0.28$, $Porosity\ Distribution\ 3$,
$e_0 = 0.3$, $FG - UU$, $W_{max}/h_{Total} = 1$

7. Conclusions

The nonlinear vibrational characteristics of sandwich cylindrical shells are considered in this study. To bring our findings closer to practical applications and align them with experimental studies, the FSDT is employed to model various points within the structure. The core of these cylindrical shells is comprised of FG porous materials, which are further reinforced with layers of nanocomposites embedded with CNTs to enhance their mechanical performance. The governing equations for nonlinear motion are derived using Hamilton's principle. Subsequently, mathematical solutions for these sandwich cylindrical shells are obtained through the application of Galerkin's and multiple-scale methods. A comprehensive comparison with prior research findings is conducted to substantiate the robustness of our results. Lastly, the influence of different parameters on the results is considered. It is generally observed that the results tend to be reduced by an increase in the porosity coefficient. However, in cases of a symmetric distribution of porosity, a slight enhancement in the results is noted. Moreover, an increase in the W_{Max}/h_{Total}

ratio leads to a significant enhancement in the results. The most and least values of the results are found to be associated with different porosity patterns, namely FG-AV and FG-VA, respectively, while the outcomes for other patterns are observed to be very close to each other. An increase in the core-to-faces thickness ratio is seen to result in a reduction in the outcomes. Additionally, due to a significant reduction in the shell's stiffness, the results are decreased. Furthermore, an enhancement in the rigidity of the structure is observed by increasing both foundation parameters, namely springs and shear layer parameters, leading to an improvement in the results.

Acknowledgment

Hunan Provincial Department of Education Project (22A0535, 20B534), Hunan Natural Science Foundation Project (2023JJ50265, 2021JJ30631), Shaoyang Science and Technology Plan Project (2022GZ1007,2021GZ040).

References

Al-Osta, M.A., Saidi, H., Tounsi, A., Al-Dulaijan, S.U., Al-Zahrani, M.M., Sharif, A. and Tounsi, A. (2021), "Influence of porosity on the hygro-thermo-mechanical bending response of an AFG ceramic-metal plates using an integral plate model", *Smart Struct. Syst.*, **28**(4), 499-513. https://doi.org/10.12989/SSS.2021.28.4.499.

Alhaifi, K., Khorshidvand, A.R., Al-Masoudy, M.M., Arshid, E. and Madani, S.H. (2023), "A shooting method for buckling and post-buckling analyses of FGSP circular plates considering various patterns of Pores' placement", *Struct. Eng. Mech.*, **85**(3), 419-432. https://doi.org/10.12989/sem.2023.85.3.419.

Alibeigloo, A. (2013), "Static analysis of functionally graded carbon nanotube-reinforced composite plate embedded in piezoelectric layers by using theory of elasticity", *Compos. Struct.*, **95**, 612-622. https://doi.org/10.1016/j.compstruct.2012.08.018.

Allahkarami, F., Nikkhah-bahrami, M. and Saryazdi, M.G. (2018), "Magneto-thermo-mechanical dynamic buckling analysis of a FG-CNTs-reinforced curved microbeam with different boundary conditions using strain gradient theory", *Int. J. Mech. Mater. Des.*, **14**(2), 243-261. https://doi.org/10.1007/s10999-017-9374-5.

Amir, S., Arshid, E. and Maraghi, Z.K. (2020a), "Free vibration analysis of magneto-rheological smart annular three-layered plates subjected to magnetic field in viscoelastic medium", *Smart Struct. Syst.*, **25**(5), 581-592. https://doi.org/10.12989/sss.2020.25.5.581.

Amir, S., Arshid, E., Rasti-Alhosseini, S.M.A. and Loghman, A. (2020b), "Quasi-3D tangential shear deformation theory for size-dependent free vibration analysis of three-layered FG porous micro rectangular plate integrated by nano-composite faces in hygrothermal environment", *J. Therm. Stress.*, **43**(2), 133-156. https://doi.org/10.1080/01495739.2019.1660601.

Aragh, B.S., Barati, A.H.N. and Hedayati, H. (2012), "Eshelby-Mori-Tanaka approach for vibrational behavior of continuously graded carbon nanotube-reinforced cylindrical panels", *Compos. Part B Eng.*, **43**(4), 1943-1954. https://doi.org/10.1016/j.compositesb.2012.01.004.

Arefi, M., Bidgoli, E.M.R. and Zenkour, A.M. (2018a), "Size-dependent free vibration and dynamic analyses of a sandwich microbeam based on higher-order sinusoidal shear deformation theory and strain gradient theory", *Smart Struct. Syst.*, **22**(1), 27-40. https://doi.org/10.12989/sss.2018.22.1.027.

Arefi, M., Mohammad-Rezaei Bidgoli, E., Dimitri, R. and Tornabene, F. (2018b), "Free vibrations of functionally graded polymer composite nanoplates reinforced with graphene nanoplatelets", *Aerosp. Sci. Technol.*, **81**, 108-117. https://doi.org/10.1016/J.AST.2018.07.036.

Arefi, M., Mohammad-Rezaei Bidgoli, E. and Rabczuk, T. (2019a), "Effect of various characteristics of graphene nanoplatelets on thermal buckling behavior of FGRC micro plate based on MCST", *Eur. J. Mech. A Solids*, **77**, 103802. https://doi.org/10.1016/j.euromechsol.2019.103802.

Arefi, M., Mohammad-Rezaei Bidgoli, E. and Rabczuk, T. (2019b), "Thermo-mechanical buckling behavior of FG GNP reinforced micro plate based on MSGT", *Thin Wall. Struct.*, **142**, 444-459. https://doi.org/10.1016/j.tws.2019.04.054.

Arshid, E., Soleimani-Javid, Z., Amir, S. and Duc, N.D. (2022), "Higher-order hygro-magneto-electro-thermomechanical analysis of FG-GNPs-reinforced composite cylindrical shells embedded in PEM layers", *Aerosp. Sci. Technol.*, **126**, 107573. https://doi.org/10.1016/j.ast.2022.107573.

Arshid, E., Amir, S. and Loghman, A. (2023a), "Thermoelastic vibration characteristics of asymmetric annular porous reinforced with nano-fillers microplates embedded in an elastic medium: CNTs Vs. GNPs", *Arch. Civil Mech. Eng.*, **23**(2), 100. https://doi.org/10.1007/s43452-023-00624-8.

Arshid, E., Amir, S. and Loghman, A. (2023b), "On the vibrations of FG GNPs-RPN annular plates with piezoelectric/metallic coatings on Kerr elastic substrate considering size dependency and surface stress effects", *Acta Mechanica*, 1-42. https://doi.org/10.1007/s00707-023-03593-4.

Arshid, E., Ghorbani, M.A., Momeni Nia, M.J., Civalek, Ö. and Kumar, A. (2023c), "Thermo-elastic buckling behaviors of advanced fluid-infiltrated porous shells integrated with GPLs-reinforced nanocomposite patches", *Mech. Adv. Mater. Struct.*, 1-17. https://doi.org/10.1080/15376494.2023.2251015.

Arshid, E., Momeni Nia, M.J., Ghorbani, M.A., Civalek, Ö. and Kumar, A. (2023d), "On the poroelastic vibrations of lightweight FGSP doubly-curved shells integrated with GNPs-reinforced composite coatings in thermal atmospheres", *Appl. Math. Modell.*, **124**, 122-141. https://doi.org/10.1016/j.apm.2023.07.036.

Arshid, E., Amir, S. and Loghman, A. (2024a), "Aero-Hygro-Thermoelastic size-dependent analysis of NCMF-reinforced GNPs sector microplates located between piezoelectric patches in supersonic flow considering surface stress effects", *Mech. Based Des. Struct.*, 1-62. https://doi.org/10.1080/15397734.2023.2295532.

Arshid, E., Amir, S., Loghman, A. and Civalek, Ö. (2024b), "Aerodynamic stability and free vibration of fgp-reinforced nano-fillers annular sector microplates exposed to supersonic flow", *Thin Wall Struct.*, 111610. https://doi.org/10.1016/j.tws.2024.111610.

Arshid, E., Azimi, M., Moradi, M., El Ouni, M. H. and Alashker, Y. (2024c), "Mathematical solution for vibrational response of shear and normal deformable advanced metal foam cmbs treated with nanocomposite actuators", *Int. J. Struct. Stabil. Dyn.*, https://doi.org/10.1142/S0219455425501184.

Babaei, M., Asemi, K. and Safarpour, P. (2019), "Buckling and static analyses of functionally graded saturated porous thick beam resting on elastic foundation based on higher order beam theory", *Iranian J. Mech. Eng. Transact. ISME*, **20**(1), 94-112.

Babaei, M., Hajmohammad, M. H. and Asemi, K. (2020), "Natural frequency and dynamic analyses of functionally graded saturated porous annular sector plate and cylindrical panel based on 3D elasticity", *Aerosp. Sci. Technol.*, **96**, 105524. https://doi.org/10.1016/j.ast.2019.105524.

Babaei, H. and Eslami, M.R. (2021), "On nonlinear vibration and snap-through buckling of long FG porous cylindrical panels using nonlocal strain gradient theory", *Compos. Struct.*, **256**, 113125. https://doi.org/10.1016/j.compstruct.2020.113125.

Babaei, M. and Asemi, K. (2022), "Stress analysis of functionally graded saturated porous rotating thick truncated cone", *Mech. Based Des. Struct.*, **50**(5), 1537-1564. https://doi.org/10.1080/15397734.2020.1753536.

Babaei, M., Kiarasi, F., Tehrani, M.S., Hamzei, A., Mohtarami, E. and Asemi, K. (2022), "Three dimensional free vibration analysis of functionally graded graphene reinforced composite laminated cylindrical panel", *Proceedings of the Institution of Mechanical Engineers, Part L: Journal of Materials: Design and Applications*, **236**(8), 1501-1514. https://doi.org/10.1177/14644207211073445.

Babaei, H., Zavari, S., Kaveh, A., Arshid, E. and Civalek, O. (2024), "Dynamic response of advanced lightweight porous plates integrated with nanocomposite face sheets resting on elastic substrate", *Int. J. Struct. Stabil. Dyn.*, Online Ready. https://doi.org/10.1142/S0219455425501329.

Berghouti, H., Bedia, E.A.A., Benkhedda, A. and Tounsi, A. (2019), "Vibration analysis of nonlocal porous nanobeams made of functionally graded material", *Adv. Nano Res.*, **7**(5), 351-364. https://doi.org/10.12989/anr.2019.7.5.351.

Bi, R., Gao, J. and Allahyari, S. (2021), "Higher order plate theory for buckling analysis of plates based on exact solution", *Steel Compos. Struct.*, **40**(3), 459. https://doi.org/10.12989/SCS.2021.40.3.451.

Bi, S., Zhang, E., Babaei, M., Tornabene, F. and Dimitri, R. (2023), "The influence of GPL reinforcements on the post-buckling behavior of FG porous rings subjected to an external pressure", *Mathematics*, **11**(11), 2421. https://doi.org/10.3390/math11112421.

Bidgoli, E.M.R. and Arefi, M. (2023), "Effect of porosity and characteristics of carbon nanotube on the nonlinear characteristics of a simply-supported sandwich plate", *Arch. Civil Mech. Eng.*, **23**(3), 214. https://doi.org/10.1007/s43452-023-00752-1.

Bidgoli, E.M.R., Arefi, M. and Mohammadimehr, M. (2022), "Free vibration analysis of honeycomb doubly curved shell integrated with CNT-reinforced piezoelectric layers", *Mech. Based Des. Struct.*, **50**(12), 4409-4440. https://doi.org/10.1080/15397734.2020.1836969.

Cong, P.H., Chien, T.M., Khoa, N.D. and Duc, N.D. (2018), "Nonlinear thermomechanical buckling and post-buckling response of porous FGM plates using Reddy's HSDT", *Aerosp. Sci. Technol.*, **77**, 419-428. https://doi.org/10.1016/j.ast.2018.03.020.

Das, Y.C. (1964), "Vibrations of orthotropic cylindrical shells", *Appl. Sci. Res. A*, **12**(4-5), 317-326. https://doi.org/10.1007/BF03185004.

Dehghan, M., Ebrahimi, F. and Vinyas, M. (2020), "Wave dispersion characteristics of fluid-conveying magneto-electro-elastic nanotubes", *Eng. Comput.*, **36**(4), 1687-1703. https://doi.org/10.1007/s00366-019-00790-5.

Djilali, N., Bousahla, A.A., Kaci, A., Selim, M.M., Bourada, F., Tounsi, A., Tounsi, A., Benrahou, K.H. and Mahmoud, S.R. (2022), "Large cylindrical deflection analysis of FG carbon nanotube-reinforced plates in thermal environment using a simple integral HSDT", *Steel Compos. Struct.*, **42**(6), 779-789. https://doi.org/10.12989/SCS.2022.42.6.779.

Dong, S.B. (1968), "Free vibration of laminated orthotropic cylindrical shells", *J. Acoust. Soc. Am.*, **44**(6), 1628-1635. https://doi.org/10.1121/1.1911306.

Dzung, N.M., Tan, N.C., Ha, N.H., Tien, N.D., Eslami, H. and Ninh, D.G. (2024), "Effects of edge-crack orientation and depth on non-linear dynamics of laminated nanocomposite single-variable-edge plates", *Eng. Struct.*, **304**, 117553. https://doi.org/10.1016/j.engstruct.2024.117553.

Forsat, M., Musharavati, F., Eltai, E., Zain, A.M., Mobayen, S. and Mohamed, A.M. (2021), "Vibration characteristics of microplates with GNPs-reinforced epoxy core bonded to piezoelectric-reinforced CNTs patches", *Adv. Nano Res.*, **11**(2), 140. https://doi.org/10.12989/ANR.2021.11.2.115.

Gao, Q., Ding, Z. and Liao, W.H. (2022), "Effective elastic properties of irregular auxetic structures", *Compos. Struct.*, **287**, 115269. https://doi.org/10.1016/j.compstruct.2022.115269.

Ha, N.H., Tan, N.C., Dzung, N.M., Long, N.T., Quan, N.M., Eslami, H. and Ninh, D.G. (2024), "A new study for dynamical characteristics of double-variable-edge and variable thickness plates made of open-cell porous metal", *Aerosp. Sci. Technol.*, **145**, 108830. https://doi.org/10.1016/j.ast.2023.108830.

Han, Q., Li, X. and Chu, F. (2018), "Skidding behavior of cylindrical roller bearings under time-variable load conditions", *Int. J. Mech. Sci.*, **135**, 203-214. https://doi.org/10.1016/j.ijmecsci.2017.11.013.

Hou, Y., Choi, K.R., Ghazouani, N., Kaveh, A., Babaei, Z. and Kumar, A. (2023), "Static package design thorough thickness stretching and thermal environment effects for porous micro-scaled plates with piezoelectric nanocomposite patches", *Acta Mechanica*, **235**(2), 1235-1254. https://doi.org/10.1007/S00707-023-03794-X/METRICS.

Jalaei, M.H. and Civalek, (2019), "On dynamic instability of magnetically embedded viscoelastic porous FG nanobeam", *Int. J. Eng. Sci.*, **143**, 14-32. https://doi.org/10.1016/j.ijengsci.2019.06.013.

Jam, J.E., Pourasghar, A. and Kamarian, S. (2012), "Effect of the aspect ratio and waviness of carbon nanotubes on the vibrational behavior of functionally graded nanocomposite cylindrical panels", *Polym. Compos.*, **33**(11), 2036-2044. https://doi.org/10.1002/pc.22346.

Jeyaraj, P. and Rajkumar, I. (2013), "Static behavior of FG-CNT polymer nano composite plate under elevated non-uniform temperature fields", *Procedia Eng.*, **64**, 825-834. https://doi.org/10.1016/j.proeng.2013.09.158.

Kalamkarov, A.L., Georgiades, A.V., Rokkam, S.K., Veedu, V.P. and Ghasemi-Nejhad, M.N. (2006), "Analytical and numerical techniques to predict carbon nanotubes properties", *Int. J. Solid Struct.*, **43**(22-23), 6832-6854. https://doi.org/10.1016/j.ijsolstr.2006.02.009.

Kargar, J., Ghorbanpour Arani, A., Arshid, E. and Irani Rahaghi, M. (2021), "Vibration analysis of spherical sandwich panels with MR fluids core and magneto-electro-elastic face sheets resting on orthotropic viscoelastic foundation", *Struct. Eng. Mech.*, **78**(5), 572. https://doi.org/10.12989/SEM.2021.78.5.557.

Kaveh, A., Babaei, H., Zavari, S., Arshid, E. and Civalek, Ö. (2024), "Vibrational response of a sandwich microplate considering the impact of flexoelectricity and based on a novel porous-FGM formulation", *Mech. Based Des. Struct.*, 1-22. https://doi.org/10.1080/15397734.2024.2337913.

Khoddami Maraghi, Z., Amir, S. and Arshid, E. (2022), "On the natural frequencies of smart circular plates with magneto-rheological fluid core embedded between magnetostrictive patches on Kerr elastic substance", *Mech. Based Des. Struct.*, 1-18. https://doi.org/10.1080/15397734.2022.2156885.

Khoddami Maraghi, Z. and Arshid, E. (2024), "On the vibrational behavior of variable thickness FG porous beams with graphene-reinforced nanocomposite facesheets", *Acta Mechanica*, https://doi.org/10.1007/s00707-024-03987-y.

Kiani, Y., Shakeri, M. and Eslami, M.R. (2012), "Thermoelastic free vibration and dynamic behaviour of an FGM doubly curved panel via the analytical hybrid Laplace-Fourier transformation", *Acta Mechanica*, **223**(6), 1199-1218.

https://doi.org/10.1007/s00707-012-0629-9.
Kiarasi, F., Babaei, M., Dimitri, R. and Tornabene, F. (2020), "Hygrothermal modeling of the buckling behavior of sandwich plates with nanocomposite face sheets resting on a Pasternak foundation", *Continuum Mech. Thermodyn.*, 1-22. https://doi.org/10.1007/s00161-020-00929-6.
Kiarasi, F., Babaei, M., Mollaei, S., Mohammadi, M. and Asemi, K. (2021), " Free vibration analysis of FG porous joined truncated conical-cylindrical shell reinforced by graphene platelets", *Adv. Nano Res.*, **11**(4), 380. https://doi.org/10.12989/ANR.2021.11.4.361.
Liu, B., Xing, Y.F., Qatu, M.S. and Ferreira, A.J.M. (2012), "Exact characteristic equations for free vibrations of thin orthotropic circular cylindrical shells", *Compos. Struct.*, **94**(2), 484-493. https://doi.org/10.1016/j.compstruct.2011.08.012.
Malekzadeh, P. and Shojaee, M. (2013), "Buckling analysis of quadrilateral laminated plates with carbon nanotubes reinforced composite layers", *Thin Wall. Struct.*, **71**, 108-118. https://doi.org/10.1016/j.tws.2013.05.008.
Mao, J.J. and Zhang, W. (2019), "Buckling and post-buckling analyses of functionally graded graphene reinforced piezo-electric plate subjected to electric potential and axial forces", *Compos. Struct.*, **216**, 392-405. https://doi.org/10.1016/j.compstruct.2019.02.095.
Mindlin, R.D. (1968), "Polarization gradient in elastic dielectrics", *Int. J. Solids Struct.*, **4**(6), 637-642. https://doi.org/10.1016/0020-7683(68)90079-6.
Mirjavadi, S.S., Forsat, M., Nia, A.F., Badnava, S., Hamouda, A.M.S., Mirjavadi, S.S., Forsat, M., Nia, A.F., Badnava, S. and Hamouda, A.M.S. (2020a), "Nonlocal strain gradient effects on forced vibrations of porous FG cylindrical nanoshells", *Adv. Nano Res.*, **8**(2), 156. https://doi.org/10.12989/ANR.2020.8.2.149.
Mirjavadi, S.S., Nikookar, M., Mollaee, S., Forsat, M., Barati, M. R., Hamouda, A.M.S., Mirjavadi, S.S., Nikookar, M., Mollaee, S., Forsat, M., Barati, M.R. and Hamouda, A.M.S. (2020b), "Analyzing exact nonlinear forced vibrations of two-phase magneto-electro-elastic nanobeams under an elliptic-type force", *Adv. Nano Res.*, **9**(1), 58. https://doi.org/10.12989/ANR.2020.9.1.047.
Mohammad-Rezaei Bidgoli, E. and Arefi, M. (2019), "Free vibration analysis of micro plate reinforced with functionally graded graphene nanoplatelets based on modified strain-gradient formulation", *J. Sandw. Struct. Mater.*, **23**(2), 436-472. https://doi.org/10.1177/1099636219839302.
Mohammad-Rezaei Bidgoli, E. and Arefi, M. (2023a), "Nonlinear vibration analysis of sandwich plates with honeycomb core and graphene nanoplatelet-reinforced face-sheets", *Arch. Civil Mech. Eng.*, **23**(1), 56. https://doi.org/10.1007/s43452-022-00589-0.
Mohammad-Rezaei Bidgoli, E. and Arefi, M. (2023b), "Size-dependent thermomechanical critical loads of GPL-reinforced nanobeams", *Waves Random Complex Med.*, 1-21. https://doi.org/10.1080/17455030.2023.2169385.
Mohammad-Rezaei Bidgoli, E. and Arefi, M. (2023c), "Dynamic results of GNPRC sandwich shells", *Steel Compos. Struct.*, **48**(3), 273. https://doi.org/10.12989/SCS.2023.48.3.263.
Mohammadimehr, M., Salemi, M. and Rousta Navi, B. (2016), "Bending, buckling, and free vibration analysis of MSGT microcomposite Reddy plate reinforced by FG-SWCNTs with temperature-dependent material properties under hydro-thermo-mechanical loadings using DQM", *Compos. Struct.*, **138**, 361-380. https://doi.org/10.1016/j.compstruct.2015.11.055.
Mohammadimehr, M., Arshid, E., Alhosseini, S.M.A.R., Amir, S. and Arani, M.R.G. (2019), "Free vibration analysis of thick cylindrical MEE composite shells reinforced CNTs with temperature-dependent properties resting on viscoelastic foundation", *Struct. Eng. Mech.*, **70**(6), 683-702. https://doi.org/10.12989/sem.2019.70.6.683.
Mousavi, S.B., Amir, S., Jafari, A. and Arshid, E. (2021), "Analytical solution for analyzing initial curvature effect on vibrational behavior of PM beams integrated with FGP layers based on trigonometric theories", *Adv. Nano Res.*, **10**(3), 235-251. https://doi.org/10.12989/anr.2021.10.3.235.
Ni, Y., Sun, J., Zhang, J., Tong, Z., Zhou, Z. and Xu, X. (2023), "Accurate buckling analysis of magneto-electro-elastic cylindrical shells subject to hygro-thermal environments", *Appl. Math. Modell.*, **118**, 798-817. https://doi.org/10.1016/j.apm.2023.02.015.
Ninh, D.G. and Bich, D.H. (2016), "Nonlinear torsional buckling and post-buckling of eccentrically stiffened ceramic functionally graded material metal layer cylindrical shell surrounded by elastic foundation subjected to thermo-mechanical load", *J. Sandw. Struct. Mater.*, **18**(6), 712-738. https://doi.org/10.1177/1099636216644787.
Ninh, D.G., Ha, N.H., Long, N.T., Tan, N.C., Tien, N.D. and Dao, D.V. (2023), "Thermal vibrations of complex-generatrix shells made of sandwich CNTRC sheets on both sides and open/closed cellular functionally graded porous core", *Thin Wall. Struct.*, **182**, 110161. https://doi.org/10.1016/j.tws.2022.110161.
Paul, R., Kumbhakar, P. and Mitra, A.K. (2013), "A facile chemical synthesis of a novel photo catalyst: SWCNT/titania nanocomposite", *Adv. Nano Res.*, **1**(2), 71-82. https://doi.org/10.12989/anr.2013.1.2.071.
Qatu, M.S. (2004), *Vibration of Laminated Shells and Plates*, In *Vibration of Laminated Shells and Plates*, Elsevier. https://doi.org/10.1016/B978-0-08-044271-6.X5000-5.
Qatu, M.S., Sullivan, R.W. and Wang, W. (2010), "Recent research advances on the dynamic analysis of composite shells: 2000-2009", *Compos. Struct.*, **93**(1), 14-31. https://doi.org/10.1016/j.compstruct.2010.05.014.
Qin, B., Wang, Q., Zhong, R., Zhao, X. and Shuai, C. (2020), "A three-dimensional solution for free vibration of FGP-GPLRC cylindrical shells resting on elastic foundations: a comparative and parametric study", *Int. J. Mech. Sci.*, **187**, 105896. https://doi.org/10.1016/j.ijmecsci.2020.105896.
Quang, V.D., Khoa, N.D. and Duc, N.D. (2021), "The effect of structural characteristics and external conditions on the dynamic behavior of shear deformable FGM porous plates in thermal environment", *J. Mech. Sci. Technol.*, **35**(8), 3323-3329. https://doi.org/10.1007/S12206-021-0706-X/METRICS.
Radić, N. (2018), "On buckling of porous double-layered FG nanoplates in the Pasternak elastic foundation based on nonlocal strain gradient elasticity", *Compos. Part B Eng.*, **153**, 465-479. https://doi.org/10.1016/j.compositesb.2018.09.014.
Safaei, B., Khoda, F.H. and Fattahi, A.M. (2019), "Non-classical plate model for single-layered graphene sheet for axial buckling", *Adv. Nano Res.*, **7**(4), 265-275. https://doi.org/10.12989/anr.2019.7.4.265.
Shen, H.S. and Xiang, Y. (2014), "Nonlinear vibration of nanotube-reinforced composite cylindrical panels resting on elastic foundations in thermal environments", *Compos. Struct.*, **111**, 291-300. https://doi.org/10.1016/j.compstruct.2014.01.010.
Shen, H.S. (2011), "Postbuckling of nanotube-reinforced composite cylindrical shells in thermal environments, Part I: Axially-loaded shells", *Compos. Struct.*, **93**(8), 2096-2108. https://doi.org/10.1016/j.compstruct.2011.02.011.
Shen, H.S. and Xiang, Y. (2012), "Nonlinear vibration of nanotube-reinforced composite cylindrical shells in thermal environments", *Comput. Meth. Appl. Mech. Eng.*, **213-216**(8), 196-205. https://doi.org/10.1016/j.cma.2011.11.025.
Shen, H.S. (2013), "Thermal buckling and postbuckling of functionally graded fiber-reinforced composite laminated plates", *J. Compos. Mater.*, **47**(22), 2783-2795.

https://doi.org/10.1177/0021998312458131.

Shen, H.S. and Xiang, Y. (2013), "Postbuckling of nanotube-reinforced composite cylindrical shells under combined axial and radial mechanical loads in thermal environment", *Compos. Part B Eng.*, **52**, 311-322. https://doi.org/10.1016/j.compositesb.2013.04.034.

Shen, H.S., Xiang, Y. and Fan, Y. (2017a), "Nonlinear vibration of functionally graded graphene-reinforced composite laminated cylindrical shells in thermal environments", *Compos. Struct.*, **182**, 447-456. https://doi.org/10.1016/j.compstruct.2017.09.010.

Shen, H.S., Xiang, Y. and Fan, Y. (2017b), "Nonlinear vibration of functionally graded graphene-reinforced composite laminated cylindrical shells in thermal environments", *Compos. Struct.*, **182**, 447-456. https://doi.org/10.1016/j.compstruct.2017.09.010.

Shen, X., Li, T., Xu, L., Kiarasi, F., Babaei, M. and Asemi, K. (2024), "Free vibration analysis of FG porous spherical cap reinforced by graphene platelet resting on Winkler foundation", *Adv. Nano Res.*, **16**(1), 26. https://doi.org/10.12989/ANR.2024.16.1.011.

Sivadas, K.R. and Ganesan, N. (1991), "Vibration analysis of laminated conical shells with variable thickness", *J. Sound Vib.*, **148**(3), 477-491. https://doi.org/10.1016/0022-460X(91)90479-4.

Sobhani, E., Masoodi, A. R., Civalek, Ö. and Avcar, M. (2022), "Natural frequency analysis of FG-GOP/ polymer nano-composite spheroid and ellipsoid doubly curved shells reinforced by transversely-isotropic carbon fibers", *Eng. Anal. Bound. Elem.*, **138**, 369-389. https://doi.org/10.1016/j.enganabound.2022.03.009.

Soleimani-Javid, Z., Arshid, E., Khorasani, M., Amir, S. and Tounsi, A. (2021), "Size-dependent flexoelectricity-based vibration characteristics of honeycomb sandwich plates with various boundary conditions", *Adv. Nano Res.*, **10**(5), 449-460. https://doi.org/10.12989/anr.2021.10.5.449.

Su, Y., Shen, Z., Long, X., Chen, C., Qi, L. and Chao, X. (2023), "Gaussian filtering method of evaluating the elastic/elasto-plastic properties of sintered nanocomposites with quasi-continuous volume distribution", *Mater. Sci. Eng. A*, **872**, 145001. https://doi.org/10.1016/j.msea.2023.145001.

Sun, L., Wang, G. and Zhang, C. (2024), "Experimental investigation of a novel high performance multi-walled carbon nano-polyvinylpyrrolidone/silicon-based shear thickening fluid damper", *J. Intell. Mater. Syst. Struct.*, **35**(6), 661-672. https://doi.org/10.1177/1045389X231222999.

Tahir, S.I., Chikh, A., Tounsi, A., Al-Osta, M.A., Al-Dulaijan, S.U. and Al-Zahrani, M.M. (2021), "Wave propagation analysis of a ceramic-metal functionally graded sandwich plate with different porosity distributions in a hygro-thermal environment", *Compos. Struct.*, **269**, 114030. https://doi.org/10.1016/j.compstruct.2021.114030.

Taj, K., Akturk, B. and Ulukaya, S. (2022), "Fresh state properties and compressive strength development of reactive MgO-based systems", *Mater. Today Proc.*, **65**, 1064-1069. https://doi.org/10.1016/j.matpr.2022.04.143.

Taj, K., Akturk, B. and Ulukaya, S. (2023a), "Influence of carbonation curing and nano-silica incorporation on compressive strength and micro-structural development of binary RMC-based systems", *J. Build. Eng.*, **66**, 105856. https://doi.org/10.1016/j.jobe.2023.105856.

Taj, K., İlcan, H., Teksin, E., Argın, G., Ardoğa, M.K., Uzal, B. and Şahmaran, M. (2023b), "Effect of duration and type of grinding on the particle size distribution and microstructure of natural pumice with low pozzolanic reactivity", *Powder Technol.*, **428**, 118839. https://doi.org/10.1016/j.powtec.2023.118839.

Tian, R., Wang, M., Zhang, Y., Jing, X. and Zhang, X. (2024), "A concave X-shaped structure supported by variable pitch springs for low-frequency vibration isolation", *Mech. Syst. Signal Pr.*, **218**, 111587. https://doi.org/10.1016/j.ymssp.2024.111587.

Tien, N.D., Hoang, V.N.V., Ninh, D.G., Huy, V.L. and& Hung, N.C. (2021), "Nonlinear dynamics and chaos of a nano-composite plate subjected to electro-thermo-mechanical loads using Flügge-Lur'e-Bryrne theory", *J. Vib. Control*, **27**(9-10), 1184-1197. https://doi.org/10.1177/1077546320938185.

Vronay, D. F. and Smith, B. L. (1970), "Free vibration of circular cylindrical shells of finite length", *AIAA J.*, **8**(3), 601-603. https://doi.org/10.2514/3.5726.

Wang, Z.X. and Shen, H.S. (2012), "Nonlinear vibration and bending of sandwich plates with nanotube-reinforced composite face sheets", *Compos. Part B Eng.*, **43**(2), 411-421. https://doi.org/10.1016/j.compositesb.2011.04.040.

Wang, H., Han, Q. and Zhou, D. (2017), "Nonlinear dynamic modeling of rotor system supported by angular contact ball bearings", *Mech. Syst. Signal Pr.*, **85**, 16-40. https://doi.org/10.1016/j.ymssp.2016.07.049.

Wang, Y.Q., Liu, Y.F. and Zu, J.W. (2019), "Size-dependent vibration of circular cylindrical polymeric microshells reinforced with graphene platelets", *Int. J. Appl. Mech.*, **11**(4). https://doi.org/10.1142/S1758825119500364.

Wang, W., Jin, Y., Mu, Y., Zhang, M. and Du, J. (2023), "A novel tubular structure with negative Poisson's ratio based on gyroid-type triply periodic minimal surfaces", *Virt. Phys. Prototyp.*, **18**(1). https://doi.org/10.1080/17452759.2023.2203701.

Yas, M.H., Pourasghar, A., Kamarian, S. and Heshmatia, M. (2013), "Three-dimensional free vibration analysis of functionally graded nanocomposite cylindrical panels reinforced by carbon nanotube", *Mater. Des.*, **49**, 583-590. https://doi.org/10.1016/j.matdes.2013.01.001.

Zavari, S., Kaveh, A., Babaei, H., Arshid, E., Dimitri, R. and Tornabene, F. (2024), "A quasi-3D hyperbolic formulation for the buckling study of metal foam microplates layered with graphene nanoplatelets-embedded nanocomposite patches with temperature fluctuations", *Compos. Struct.*, 117876. https://doi.org/10.1016/j.compstruct.2024.117876.

Zeng, S., Wang, B.L. and Wang, K.F. (2019), "Nonlinear vibration of piezoelectric sandwich nanoplates with functionally graded porous core with consideration of flexoelectric effect", *Compos. Struct.*, **207**, 340-351. https://doi.org/10.1016/j.compstruct.2018.09.040.

Zhao, J., Xie, F., Wang, A., Shuai, C., Tang, J. and Wang, Q. (2019), "Vibration behavior of the functionally graded porous (FGP) doubly-curved panels and shells of revolution by using a semi-analytical method", *Compos. Part B Eng.*, **157**, 219-238. https://doi.org/10.1016/j.compositesb.2018.08.087.

CC